Microwave and Millimeter Wave Forward Modeling Results from the 2004 North Slope of Alaska Arctic Winter Radiometric Experiment

E.R. Westwater, D. Cimini, M. Klein, and V. Leuski
Cooperative Institute for Research in Environmental Sciences
University of Colorado/NOAA-Environmental Technology Laboratory
Boulder, Colorado

V. Mattioli
Dipartimento di Ingegneria Elettronica e dell'Informazione
Universitά di Perugia
Perugia, Italy

A.J. Gasiewski
NOAA-Environmental Technology Laboratory
Boulder, Colorado

S. Dowlatshahi
Science and Technology Corporation
Boulder, Colorado

J.S. Liljegren and B.M. Lesht
Department of Energy/Argonne National Laboratory
Argonne, Illinois

J.A. Shaw
Department of Electrical and Computer Engineering
Montana State University
Bozeman, Montana

Introduction

The 2004 Arctic Winter Radiometric Experiment was conducted at the North Slope of Alaska (NSA) Atmospheric Radiation Measurement (ARM) Program's North Slope of Alaska (NSA) site near Barrow, Alaska, from March 9 to April 9, 2004. The goals of the experiment were to study the microwave and millimeter wave radiometric response to water vapor and clouds during cold and dry conditions, to obtain data for forward model studies at frequencies ranging from 22.235 – 400 GHz, to demonstrate Environmental Technology Laboratory's (ETL's) new radiometric receiver and calibration technology, and to compare radiometric and in situ water vapor measurements. A description of the experiment and

preliminary data is given by Westwater et al. (2004). A complete description of ETL's ground-based scanning radiometer (GSR) is given by Cimini et al. (2005), and a comparison of in situ radiosonde data with data from the dual-channel ARM microwave radiometer and the 12-channel ARM Microwave Radiometer Profiler (MWRP) is given by Mattioli et al. (2005). Another paper describing initial results from this experiment is given by Dowlatshahi et al. (2005). In this paper, as a necessary step in improving water vapor measurements at low concentrations, we give our results of clear sky forward model comparisons for radiometric channels near the 183.31-GHz water vapor line. Table 1 summarizes the instruments used for the studies in this paper. We also present data examples from an infrared cloud imager (ICI; Thurairajah and Shaw 2005) that, in addition to its application to cloud research, has the potential for studying the effects of clouds within a radiometer's beam.

Table 1. The subset of instruments deployed during the NSA 2004 Arctic Winter Radiometric Experiment whose data are shown here. T-temperature. ρ_V-water vapor density. RH-relative humidity. P-pressure. Z-altitude. CBT-cloud base temperature.

INSTRUMENT	FREQUENCY (GHz)	PARAMETER
ETL GSR	183.31 (±0.5,±1,±3,±5,±7,±12,±16)	PWV, ρ_V (z)
MSU ICI	8-14 μm	Cloud Images, statistics
ARM MWRP	10 μm	CBT
RADIOSONDE	LAUNCH FREQUENCY	PARAMETER
ARM Dplx	4 per day	T(z), RH(z), P(z)
ARM GW	1 per day	T(z), RH(z), P(z)
NASA SW	8 total	T(z), RH(z), P(z)

Clear Air Forward Model Studies Based on Vaisala RS-90 and Chilled Mirror Radiosondes

As discussed by Mattioli et al. (2005), Vaisala RS90 radiosondes were launched four times per day from the ARM Duplex and once per day from the location of all of the ARM instruments, the "Great White." Eight chilled mirror "Snow White" radiosondes were launched from the Duplex on the same balloons that carried the Vaisala RS90 humidity sensor. In addition to these data, we acquired synoptic soundings from the National Oceanic and Atmospheric Administration (NOAA)/National Weather Service (NWS) launches in Barrow. Mattioli et al. (2005) contains a more complete discussion of each of the humidity sensors used on the radiosonde launches. Because of substantial differences between NWS and Vaisala radiosondes, and because we suspect the NWS upper-level humidity data are incorrect, our statistical analysis here does not include the NWS radiosondes. However, to give an idea of the differences that may arise between simultaneous radiosondes, one of our typical comparisons is shown in Figure 1. It is seen that significant differences in relative humidity (RH) exist, especially above 6-8 km. A complete radiosonde statistical analysis for this experiment is given by Mattioli et al. (2005).

Our basic forward model studies involve comparing calibrated brightness temperatures (T_B) from GSR measurements (Cimini et al. 2005) with T_B calculated from radiosondes using five clear-air absorption models: (1) Liebe and Layton (1987)-LBE87, (2) Liebe et al. 1993- LBE93, (3) Rosenkranz (1998, 1999) - ROS98, (4) Rosenkranz (2003)-ROS03, and (5) Liljegren et al. (2005)-LIL05. An example of chilled mirror radiosonde calculations from Figure 1 is shown in Figure 2. In the right-hand figure, we see that around the 183.31-GHz line, differences can be as large as 15 K.

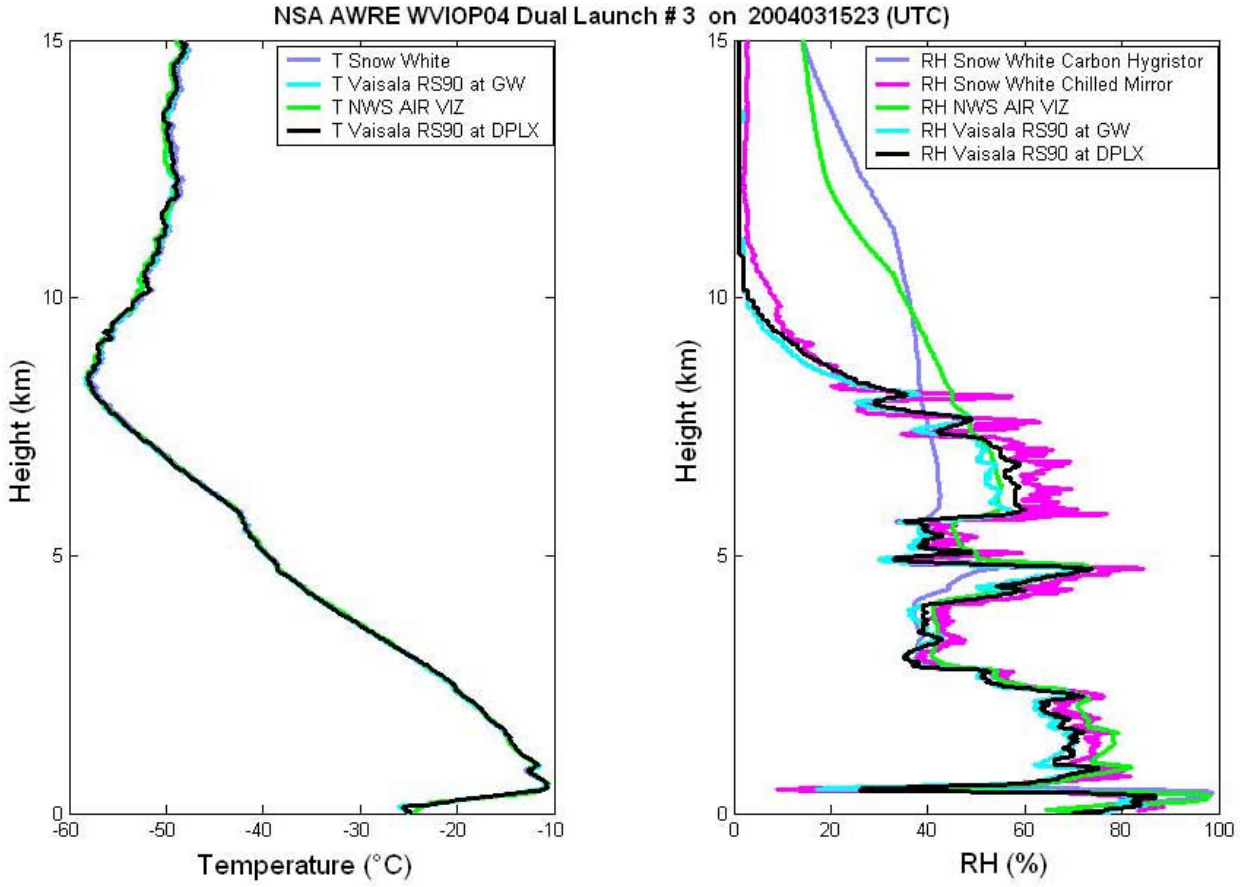

Figure 1. Comparison of temperature and RH measurements from five simultaneous radiosonde launches near Barrow, Alaska, on March 15, 2004, 2300 UTC. The NWS AIR VIZ and the Snow White Carbon Hygristor measure RH using resistors. The Vaisala RS90 uses capacitative measurements of RH, and the chilled mirror measures frost point temperature.

The T_B calculations shown in Figure 2 are monochromatic. To compare such calculations with measurements, the frequency response characteristics of each channel must be taken into account. For the GSR channels near 183.31 GHz, a double-sided bandpass must be used. Two representative bandpass filter functions, as supplied by the manufacturer, are shown in Figure 3. For each of our T_B estimates, about 1000 monochromatic calculations were averaged to yield the double-sided average.

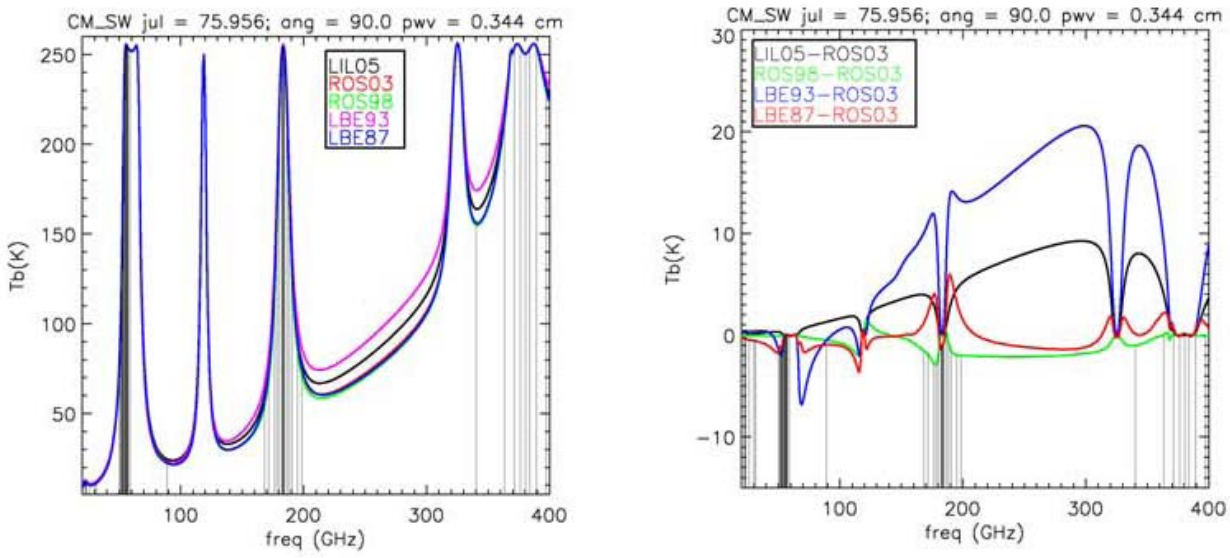

Figure 2. Comparison of forward model calculations for the chilled mirror radiosonde shown in Figure 1. Left: Absolute values of T_B calculations. Right: Differences in T_B calculations relative to of ROS03 calculations.

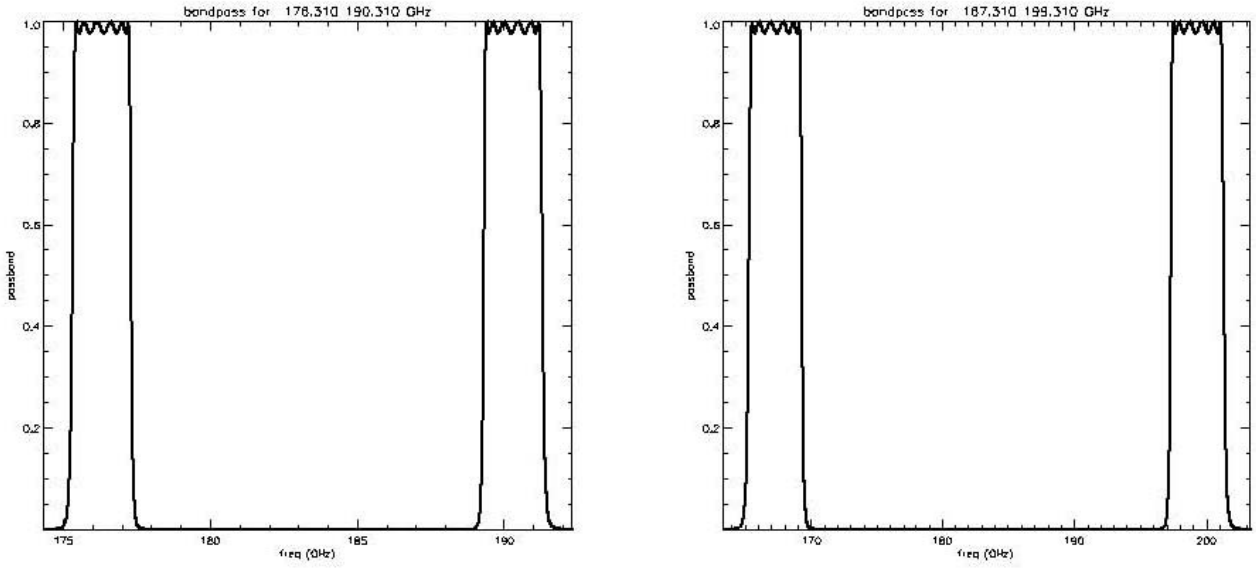

Figure 3. Examples of double-sided frequency filters for the GSR channels 183.31 ± 7 and 183.31 ± 16 GHz.

To compare measured GSR data with the model calculations, we removed outliers from the radiometric data by applying a 9-point median filter to the raw data and identified cloudy conditions using the MWRP infrared (IR) channel. For subsequent comparisons with radiosondes, 10-minute data averages were constructed. Only data with the IR clear sky threshold of T_B = 223.2 K were used. An example of our data for Julian day 73 (March 13, 2004) is shown in Figure 4.

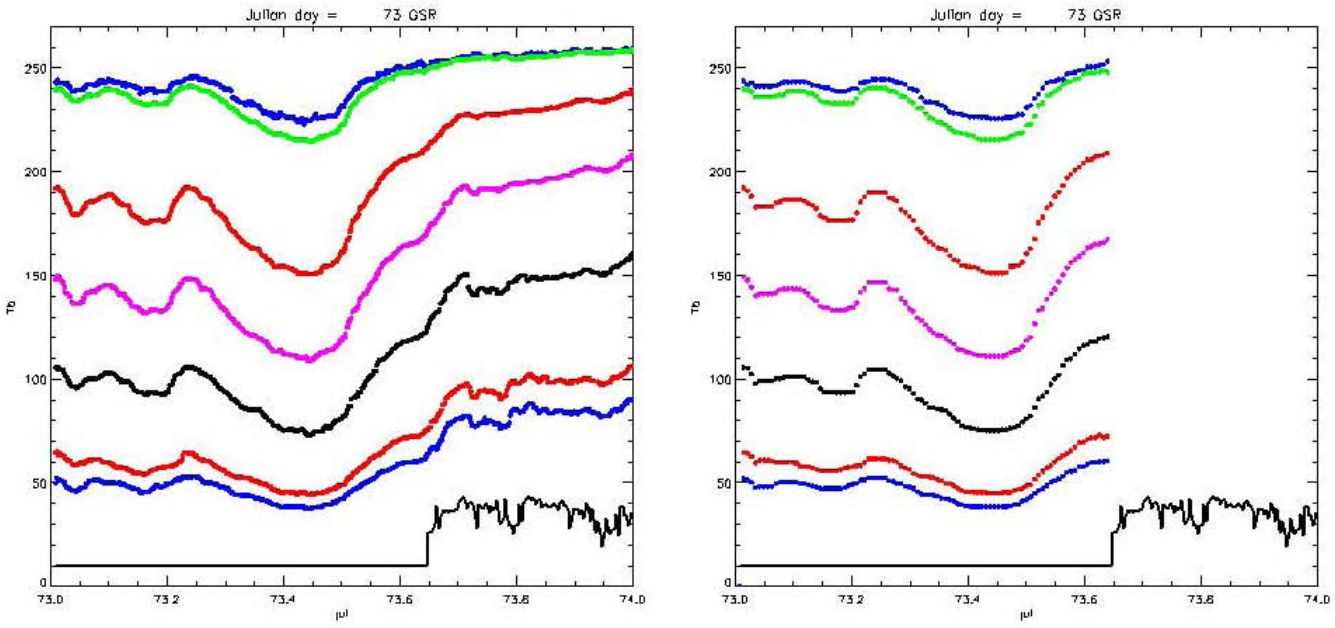

Figure 4. Left: GSR and MWRP data. Lower black curve is IR T_B from MWRP offset to 10 K from the clear condition value of 223.2 K. From bottom blue curve up, the GSR channels are arranged in increasing frequency (183.31 + [±0.5, ±1, ±3, ±5, ±7, ±12,±16 GHz]). Right: 10-minute averages of GSR data during clear conditions. Cloud cleaning was achieved using IR T_B from the MWRP shown in the lower black curve.

We have made detailed statistical comparisons between all five models and all of the available radiosonde types and locations. In Table 2, we show only the results of calculations based on RS90 radiosonde data taken at the Duplex using LBE87, LBE93, ROS98, ROS03, and LIL05. We note that there is a maximum bias of less than 1.8 K for LIL05 and 3.5 K for ROS03. In terms of bias, ROS03 is generally slightly better than LIL05. The maximum root mean square (rms) difference for LIL05 is about 4 K, and it is about 5 K for ROS03. ROS98, ROS03, and LIL05 seem to agree very well for the three opaque channels (within 1K), while LBE87 and LBE93 show alternatively large biases (all values from 1 – 6 K). For more transparent channels, LBE93 is substantially at variance with the measurements. In contrast, LIL05 stays within 1.8 K, which would support the choice of the MT_CKD continuum; conversely, LBE87 does not behave badly either (within 2.2 K). It should be clear that these rms values reflect not only model differences but also calibration and radiosonde errors. Of the latter two error sources, we believe that radiosonde errors are the most important.

Table 2. Comparison of GSR measurements with five forward models calculated from Vaisala RS90 radiosondes (N=83) that were launched at the ARM Duplex. The model with the smallest bias is highlighted in red.

Frequency - 183.31 GHz	MODEL	BIAS(K) calc-meas	STD(K)	SLOPE β Calc=α +β meas	INTERCEPT α (K)
± 0.55	LBE87	-3.76	3.98	1.12	-30.70
	LBE93	-0.34	2.26	1.03	-8.19
	ROS98	-0.59	2.37	1.04	-10.29
	ROS03	-1.03	2.49	1.05	-12.76
	LIL05	-0.80	2.39	1.04	-11.08
± 1	LBE87	-2.39	3.27	1.07	-18.60
	LBE93	1.28	2.24	1.00	0.87
	ROS98	0.27	2.35	1.02	-4.79
	ROS03	-0.03	2.36	1.03	-5.90
	LIL05	0.26	2.30	1.02	-4.22
± 3	LBE87	1.19	3.55	1.04	-5.56
	LBE93	6.08	3.43	1.01	4.19
	ROS98	-1.09	3.76	1.04	-9.05
	ROS03	-0.10	3.53	1.04	-6.64
	LIL05	0.85	3.43	1.03	-4.80
± 4.7	LBE87	-0.23	3.87	1.04	-6.45
	LBE93	5.46	3.94	1.04	-0.11
	ROS98	-5.16	3.72	1.04	-10.30
	ROS03	-3.43	3.56	1.03	-7.83
	LIL05	-1.78	3.54	1.03	-6.13
± 7	LBE87	2.20	4.02	1.06	-3.78
	LBE93	8.77	4.87	1.08	0.47
	ROS98	-3.18	3.16	1.02	-5.60
	ROS03	-1.15	3.15	1.02	-3.50
	LIL05	1.28	3.35	1.03	-2.11
± 12	LBE87	-0.04	3.52	1.10	-6.46
	LBE93	7.62	5.74	1.18	-4.23
	ROS98	-3.49	2.35	1.04	-6.26
	ROS03	-1.60	2.37	1.04	-4.48
	LIL05	1.66	3.14	1.08	-3.74
± 16	LBE87	-1.89	2.51	1.07	-5.90
	LBE93	6.18	5.06	1.20	-4.43
	ROS98	-4.21	1.82	1.02	-5.37
	ROS03	-2.49	1.83	1.02	-3.68
	LIL05	1.06	2.56	1.08	-3.24

In Figure 5 (and in the remainder of this paper), we will only show detailed comparisons with LIL05. We note that the biases are generally of the order of 1-3 K with a range of variation in T_B of some 100 to 150 K. An exception is for the 183.31 ± 4.7 GHz, which, for the Great White, has a bias of almost 7 K. In addition, for a given model, there is a considerable variation of all of the statistical parameters between each of the three radiosonde types or location. Because roughly 75% of the Duplex radiosondes were not taken simultaneously with those of the Great White, we extracted those from the Duplex radiosondes that were taken within 20 minutes of the Great White. The results of these comparisons are shown in Figure 6. We note that there is still a large bias at 183.31 ± 4.7 GHz, but the differences between the two radiosonde calculations are much smaller, being of the order of 1 – 1.5 K. Mattioli et al. (2005) shows that the precipitable water vapor difference between the simultaneous radiosondes (daytime only) at the two locations was 0.005 cm.

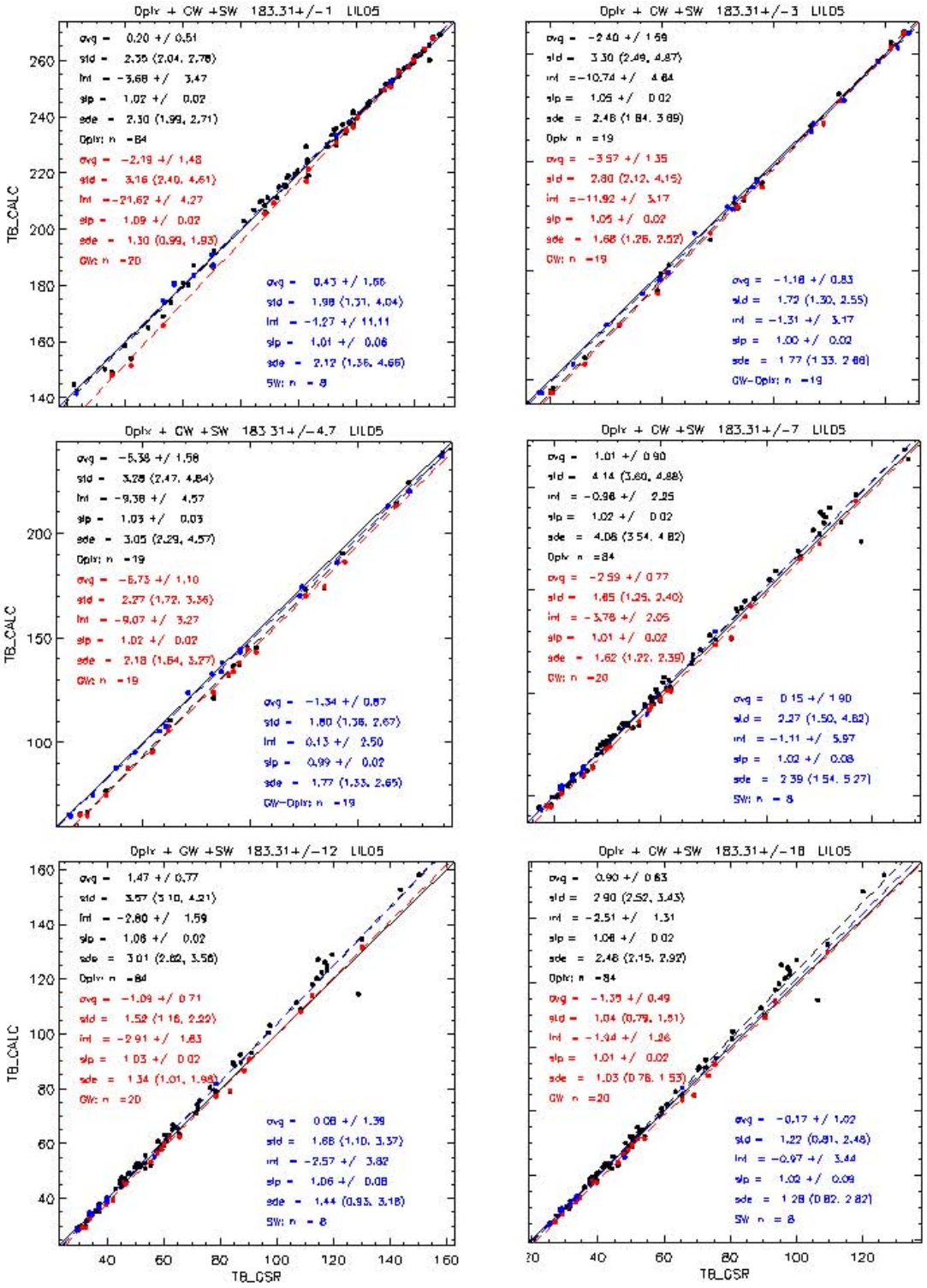

Figure 5. Comparisons of T_B model calculations with GSR measurements for the model by Liljegren et al. (2005). All comparisons refer to calculations minus measurements. The 95% confidence intervals are also shown. Duplex (RS90) comparisons are in black, Great White (RS90) in red, and Duplex (Snow White) in blue.

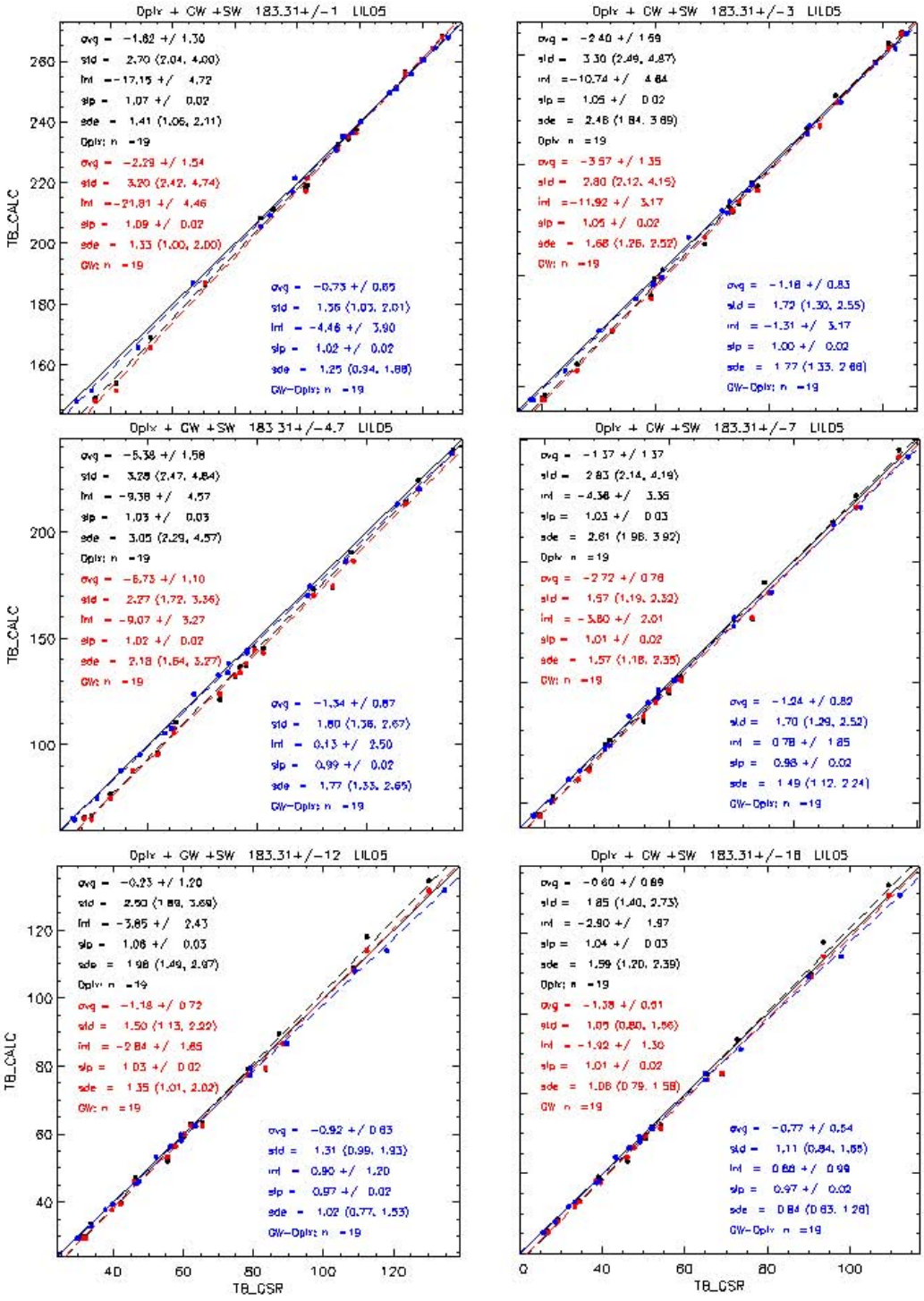

Figure 6. Comparisons of T_B model calculations with GSR measurements for the model by Liljegren et al. (2005) and for nearly simultaneous radiosonde launches at the Duplex and at the Great White. All comparisons refer to calculations minus measurements. The 95% confidence intervals are also shown. Duplex (RS90) comparisons are in black, Great White (RS90) in red, and statistics of the Great White minus the Duplex in blue.

Infrared Cloud Imager Observations

As part of this experiment, we deployed the ICI, a thermal infrared sensor that measures spatial cloud statistics from downwelling atmospheric radiance in the 8-14 μm spectral band (Thurairajah and Shaw 2005). Figure 7 shows two example ICI images recorded during March 2005 at the NSA site, indicating the cold equivalent brightness temperature of the clouds and clear sky. At NSA, the sky tends to be significantly cloudy or clear, with short transition periods of broken cloudiness. The ICI images are used to identify clear and cloudy periods, to identify brief sporadic clouds, and to investigate the variation of microwave and millimeter wave radiometer signals as a function of cloudiness within the radiometers' fields of view.

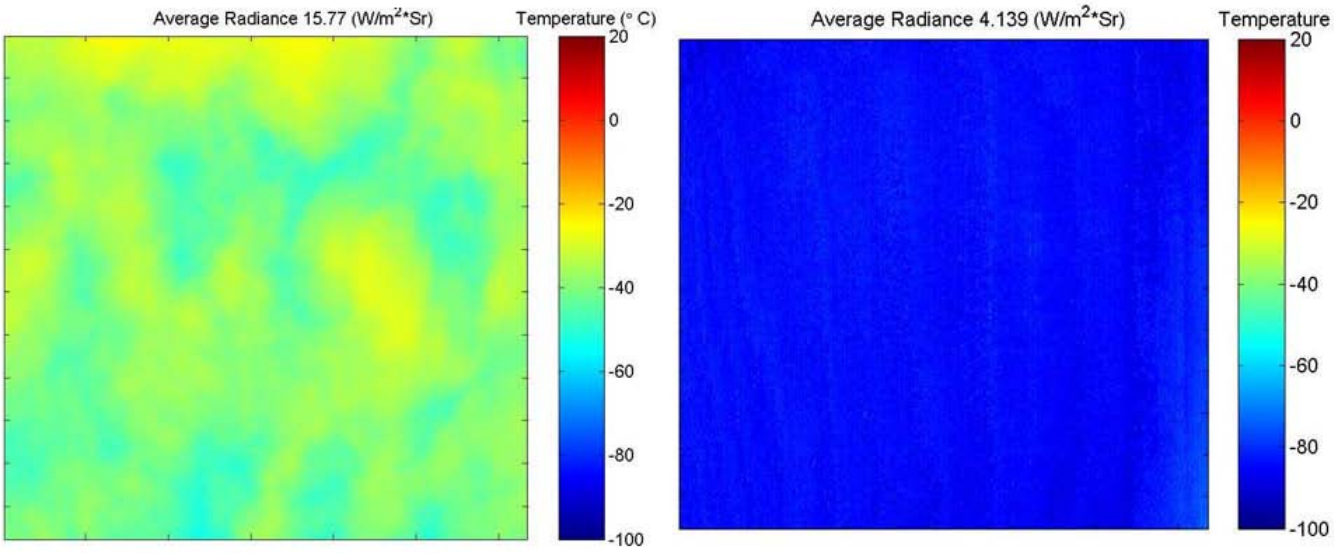

Figure 7. ICI radiometric sky images showing (left) broken low clouds and (right) clear sky. The color bar indicates equivalent band-average brightness temperature in degrees Celsius (ICI images are recorded in radiance, but displayed here in brightness temperature for convenience).

Conclusions

For clear air conditions, we have compared calibrated GSR measurements near 183.31 GHz with RTE calculations based on five absorption models. Of the five, the models by Liljegren et al. (2005) and Rosenkranz (2003) appear to be the most accurate over all of the channels. With this model, comparisons with measurements were generally with 3-4 K rms. As shown by comparisons with two simultaneous radiosondes, it appears that radiosonde errors still form a considerable portion of this error. However, because these measurements are highly sensitive to water vapor, a relative accuracy of about 2-3% is expected. This accuracy of GSR and forward models will substantially improve measurements of water vapor at low concentrations.

Future Plans

- Conduct forward model studies at other channels
- Derive meteorological products from GSR data
- Use combined active-passive retrieval of meteorological products
- Use ICI image data to investigate the effect of variable clouds within the mm-wave radiometer field of view
- Determine the information content of angular scan data

References

Cimini, D, AJ Gasiewski, M Klein, ER Westwater, V Leuski, and S Dowlatshahi. 2005. "Ground-based Scanning Radiometer Measurements during the Water Vapor IOP 2004: a valuable new data set for the study of the Arctic atmosphere." In *Proceedings of the Fifteenth ARM Science Team Meeting*, Daytona Beach, Florida, March 14-18.

Dowlatshahi, SG, AJ Gasiewski, T Uttal, M Klein, ER Westwater, and D Cimini. 2005. "Detection of Arctic Cloud Ice Properties Using Submillimeter-wave Radiometers." In *Proceedings of the Eighth Conference on Polar Meteorology and Oceanography, 85th AMS Annual Meeting*, January 9-13.

Liebe, HJ and DH Layton. 1987. "Millimeter Wave Properties Of The Atmosphere: Laboratory Studies And Propagation Modeling," National Telecommunications and Information Administration (NTIA) Report 87-24, 74 pp. (available from the National Technical Information Service, 5285 Port Royal Road, Springfield, Virginia 22161).

Liebe, HJ, GA Hufford, and MG Cotton. 1993. "Propagation modeling of moist air and suspended water/ice particles at frequencies below 1000 GHz," AGARD conference proceedings 542, 3.1–3.10.

Liljegren, JC, SA Boukabara, K Cady-Pereiria, and SA Clough. 2005. "The Effect of the Half-Width of the 22-GHz Water Vapor Line on Retrievals of Temperature and Water Vapor Profiles with a Twelve-Channel Microwave Radiometer." *IEEE Transactions on Geoscience and Remote Sensing* 43(5), 1102-1108.

Mattioli, V, ER Westwater, D Cimini, JS Liljegren, BM Lesht, S Gutman, and F Schmidlin. 2005. "Analysis of Radiosonde and PWV data from the 2004 North Slope of Alaska Arctic Winter Radiometric Experiment." In *Proceedings of the Fifteenth ARM Science Team Meeting*, Daytona Beach, Florida, March 14-18.

Rosenkranz, PW. 1998. "Water vapor microwave continuum absorption: a comparison of measurements and models." *Radio Science* 33, 919-928.

Rosenkranz, PW. 1999. Correction to "Water vapor microwave continuum absorption: a comparison of measurements and models." *Radio Science* 34(4), 1025, 1999.

Thurairajah, B and JA Shaw. 2005. "Cloud Statistics Measured with the Infrared Cloud Imager." *IEEE Transactions of the Geoscience Remote Sensings* (in press).

Westwater, ER, M Klein, A Gasiewski, V Leuski, JA Shaw, V Mattioli, D Cimini, JC Liljegren, BM Lesht, BD Zak, T Uttal, DA Hazen, BL Weber, and S Dowlatshahi. 2004. "The 2004 North Slope of Alaska Arctic Winter Radiometric Experiment." In *Proceedings of Fourteenth ARM Science Team Meeting*. March 22-26, Albuquerque, New Mexico. h [Available on-line at: http://www.arm.gov/publications/proceedings/conf14/extended_abs/westwater-er.pdf].